Earth and Planetary Science Letters 296 (2010) 403–412

Contents lists available at ScienceDirect

Earth and Planetary Science Letters

journal homepage: www.elsevier.com/locate/epsl

The influence of MORB and harzburgite composition on thermo-chemical mantle convection in a 3-D spherical shell with self-consistently calculated mineral physics

Takashi Nakagawa [a,*], Paul J. Tackley [a], Frederic Deschamps [a], James A.D. Connolly [b]

[a] Institute of Geophysics, ETH Zurich, Sonneggstrasse 5, CH-8092 Zürich, Switzerland
[b] Institute of Geochemistry and Petrology, ETH Zurich, Sonneggstrasse 5, CH-8092 Zürich, Switzerland

ARTICLE INFO

Article history:
Received 4 December 2009
Received in revised form 20 May 2010
Accepted 22 May 2010
Available online 11 June 2010

Editor: L. Stixrude

Keywords:
thermo-chemical mantle convection
seismic tomography
MORB composition
NCFMAS
mantle layering

ABSTRACT

Three-dimensional thermo-chemical mantle convection simulations with mineral assemblages self-consistently calculated using free energy minimization are used to check the sensitivity of model behavior to the assumed compositions of mid-ocean ridge basalt (MORB) and harzburgite. In addition to five-oxide $CaO–FeO–MgO–Al_2O_3–SiO_2$ (CFMAS) compositions, we test the effect of a more realistic compositional model by adding a sixth oxide Na_2O (NCFMAS) with three compositions. Results indicate that thermo-chemical structures are quite sensitive to variations in MORB composition of the order 1–2% oxide fraction, particularly FeO and Al_2O_3. Differences occur in (i) the amount of compositional stratification around 660 km depth caused by the inversion of the MORB-harzburgite density difference between 660 and 740 km depth, which is different in magnitude and depth extent between the different tested compositions, and (ii) in the degree of MORB segregation above the CMB, which is related to differences in the MORB-harzburgite density difference in the deep mantle. While improving the realism of the model by including Na_2O tends to reduce the MORB-harzburgite density difference at most pressure and temperature conditions, the differences in behavior among three NCFMAS compositions are at least as large as between either NCFMAS and the CFMAS composition, and are also related to differences in the (pressure and temperature) stability range of the post-perovskite phase between the different compositions. Comparing model spectra to those of seismic tomography using spectral heterogeneity maps, NCFMAS compositions provide a better match to seismic tomography but in all cases there is too much heterogeneity at mid lower mantle depths compared to typical seismic tomographic models, which implies that less CMB basalt segregation occurs in Earth than in the convection models.

1. Introduction

In mantle convection studies, the normal practice has been to insert a few major phase transitions by hand. Actual phase diagrams for mantle rocks are, however, quite complicated, particularly if compositional variations are taken into account, so an approach that is preferable to increasingly complicated ad hoc parameterisations is to simply calculate the stable phase assemblage and resulting physical properties as a function of temperature, pressure and composition, using the principle of minimization of free energy. This approach has been taken in two recent global mantle convection studies that have investigated the resulting seismological structures in the deep mantle, either for thermal convection (Schuberth et al., 2009) or for both thermal and thermo-chemical convections (Nakagawa et al., 2009). In these studies, the bulk composition of mantle rocks was specified as the ratio of five oxides, the so-called CFMAS system ($CaO–FeO–MgO–Al_2O_3–SiO_2$), and stable mineral assemblages were calculated as a function of temperature and hydrostatic pressure (mapped to mantle depth). However, it has become clear that for subducted mid-ocean ridge basalt (MORB) it may be important to also include the sixth most important oxide, i.e., that of sodium, Na_2O, because it can have an effect on density, just as alumina does (e.g. Xu et al., 2008). Thus, we here test the effect of this sixth oxide compared to the CFMAS system assumed in our previous study (Nakagawa et al., 2009), as well as updating the database of thermodynamic properties to that of Xu et al. (2008).

An additional complexity is that neither MORB nor harzburgite has a single composition, giving some uncertainty as to what exact composition to use in global flow calculations, and this is problematic because small changes in sodium and aluminum content affect the compressibility, and hence the density difference between MORB and harzburgite (e.g., Weidner and Wang, 1998), which is the critical property in controlling the resulting dynamics. Dynamical calculations have indicated two major effects that are strongly influenced by the density difference between MORB and harzburgite (or pyrolite), and the pressure-dependence of this density difference. One is, segregation of subducted crust above the CMB (e.g., Christensen and Hofmann, 1994; Davies, 2002; Nakagawa and

* Corresponding author.
E-mail address: ntakashi@ethz.ch (T. Nakagawa).

0012-821X/$ – see front matter © 2010 Elsevier B.V. All rights reserved.
doi:10.1016/j.epsl.2010.05.026

Tackley, 2005a,b; Brandenburg et al., 2008), which is one mechanism for building accumulations ('piles') of dense material above the CMB as indicated by seismological inversions (e.g., Ishii and Tromp, 1999; Trampert et al., 2004). The other effect is the trapping of basalt above 660 km and the trapping of harzburgite below 660 km caused by the greater depth (pressure) at which basalt transforms to perovskite, causing basalt to be less dense than harzburgite for ~tens km below 660 km, rather than more dense, which it is at most other pressures. This dynamically-induced layering, which we here refer to as the 'basalt filter effect', following the 'filter effect' term coined by Weinstein (1992), has long been proposed to occur (e.g. Irifune and Ringwood, 1993), and has been observed in a number of mantle convection calculations (Ogawa, 2000,2003; Nakagawa and Buffett, 2005; Tackley et al, 2005; Davies, 2008). A viscosity jump caused by the phase transitions near 660 km depth may also, in some cases, cause a higher concentration of basalt above and below itself (Davies, 2002; Brandenburg and van Keken, 2007), although the exact mechanism for this is not well understood.

We here apply this recent progress in calculating phase relationships by free energy minimization to investigate the effect of assumed composition in thermo-chemical mantle convection simulations in a 3-D spherical shell. We investigate the sensitivities of the resulting dynamics and structure, particularly around 660 km and near the CMB, to uncertainties in the composition of MORB and harzburgite, with MORB composition being the most important. For MORB, the influence of assuming 6 oxides (including sodium) is likely to have an effect on the density variation between MORB and harzbugite.

2. Bulk composition of mantle rocks

The bulk composition of mantle rocks has been estimated from chemical analyses of rock samples (e.g., Ringwood and Irifune, 1988; Workman and Hart, 2005; Lyubetskaya and Korenaga, 2007) as well as by trying to match seismological profiles of the mantle using mineral physics constraints (Ricard et al., 2005; Xu et al., 2008; Ganguly et al., 2009; Khan et al., 2009). On the basis of these efforts, we define mantle composition as a mixture between a harzburgite and a basalt (MORB) endmember and explore the consequences of the choices for the endmember compositions (Table 1). Following Xu et al. (2008), physical properties within the mantle are taken as the arithmetic mean of the properties of the harzburgite and MORB endmembers, which are a function of pressure and temperature. This approach represents the limiting case that the mantle is composed of a mechanical mixture of such rocks, but that this mixing occurs on a length scale that is much smaller than seismic wavelengths or the representative elements of our thermomechanical model. The elastic moduli necessary for the computation of seismic velocities are estimated by the arithmetic mean of the Voigt–Reuss–Hill averages for the harzburgite and MORB endmembers. Mantle thermodynamic properties, including elastic moduli, are computed as a function of pressure and temperature with the Perple_X free energy minimization program (Connolly, 2005) using the data of Xu et al. (2008), which is based on the thermodynamic formulation of Stixrude and Lithgow-Bertelloni (2005).

In the "improved CFMAS" system, here abbreviated to CFMAS-I, the compositions come from Ricard et al. (2005), who use the MORB composition of Ringwood and Irifune (1988) and the harzburgite composition of Ringwood (1982). The 'improvement' (relative to Nakagawa et al., 2009) refers to the use of the Xu et al. (2008) thermodynamic database. The compositions used by Xu et al (2008), here abbreviated to NCFMAS-X, are the basalt composition of Workman and Hart (2005) and a harzburgite composition that is modified from Baker and Beckett (1999) based on mass and phase balance. The compositions used in Khan et al. (2009) are from (Taylor and McLennan, 2008), and are abbreviated as NCFMAS-KT. The compositions used in Ganguly et al. (2009) are from Takahashi (1986) for harzburgite and for basalt are based on a mixture of two compositions, from Brown and Mussett (1981) for oceanic basalt and Ringwood and Irifune (1988) for MORB. A mixture of their harzburgite and MORB compositions is similar to the pyrolite composition (Ringwood, 1982). Their compositions are abbreviated as NCFMAS-G.

Of most interest here is the density difference between harzburgite and MORB, which is shown as a function of depth and temperature in Fig. 1. Fig. 1 also shows the difference between MORB and pyrolite, with pyrolite here taken to be a mechanical mixture of 80 vol.% harzburgite and 20% MORB. The density differences indicate that including Na_2O leads to a lower calculated density anomaly of MORB over most (P, T) conditions. The MORB density anomaly (relative to harzburgite) in the lower mantle is approximately 4% for the CFMAS-I compositions and close to 3% for NCFMAS-X and NCFMAS-KT. However, for NCFMAS-G the MORB density anomaly is more than 5% because of the enhanced fraction of iron in the MORB composition of NCFMAS-G (see Table 1). The density crossover below 660 km due to the different phase transition depths of the post-spinel and post-garnet transition is also clearly visible and the amplitude and depth extent depend on the composition assumed. The range of temperature and depth of this region is not very different among three NCFMAS compositions but the density crossover region of CFMAS system is slightly narrower than those of the NCFMAS system.

Plotting the density difference along an isotherm of 1800 K helps to quantify these differences, as shown in Fig. 2 for the four compositions. With CFMAS-I, MORB is denser than harzburgite everywhere except near the surface and between about 660 and 740 km depth. With NCFMAS-X the profiles are very similar but with a smaller density contrast of MORB compared to harzburgite at most depths, and NCFMAS-KT is very similar to this. With NCFMAS-G, the density difference throughout the lower mantle is the largest at around 5%, as also indicated in Fig. 1, because this MORB composition has a large amount of iron. For comparison, the experimental study of Hirose et al. (2005) found a density contrast of about 4% relative to PREM.

The post-perovskite transition is also noticeable close to the CMB, but varies widely between the different assumed compositions; for example it is less visible in the 6-oxide systems and in particular is not picked up using NCFMAS-X. In order to get the transition to occur at a consistent depth for the different compositions it would be necessary to 'tune' the thermodynamic database used in Perple_X, which we here make no attempt to do because dynamics and structures related to post-perovskite are not a focus of the present paper. The MORB density anomaly in the deepest mantle is influenced by this; for example in the improved CFMAS system the contrast is decreased close to the CMB but increased some distance above the CMB, at medium to low temperatures.

Table 1
Bulk compositions of MORB and harzburgite in molar %.

	CFMAS-I (improved)		NCFMAS-KT: Khan et al. (2009)		NCFMAS-X: Xu et al. (2008)		NCFMAS-G: Ganguly et al. (2009)	
	harz	MORB	harz	MORB	harz	MORB	harz	MORB
CaO	0.9	14.8	0.4	12.74	0.81	13.88	0.07	11.32
FeO	5.4	7.0	5.63	6.66	6.07	7.06	4.81	8.31
MgO	56.6	15.8	56.07	16.39	56.51	14.94	60.49	17.96
Al_2O_3	0.7	10.2	0.28	9.85	0.53	10.19	0.24	9.45
SiO_2	36.4	52.2	37.62	52.47	36.07	51.75	34.39	50.83
Na_2O	N/A	N/A	0.0	1.88	0.0	2.18	0.0	1.88

3. Mantle convection modeling

Using the densities presented in the previous section as well as other physical parameters calculated using Perple_X, we have simulated thermo-chemical mantle convection over the age of the Earth. The model assumes the compressible, truncated anelastic approximation and

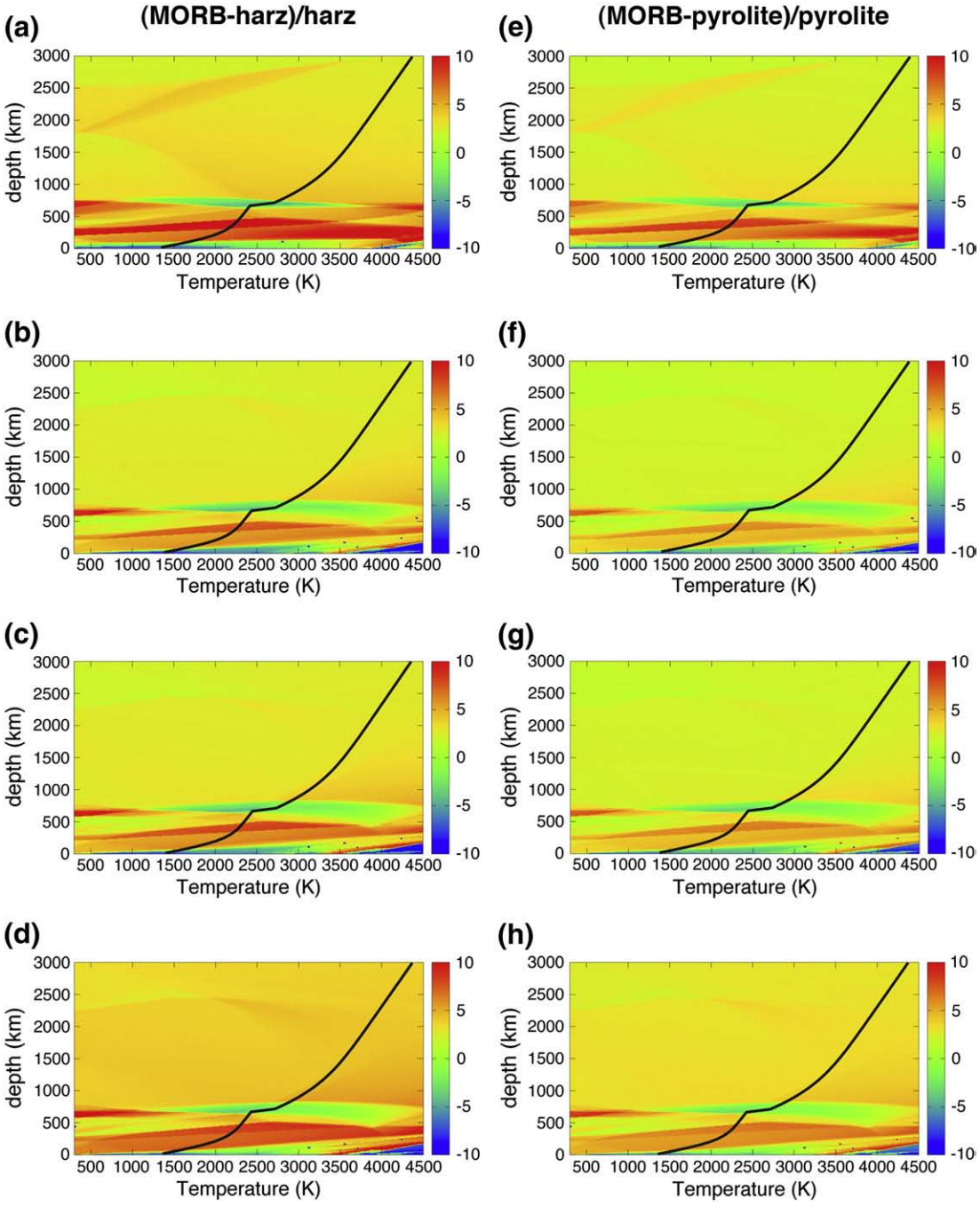

Fig. 1. Density difference maps computed by Perple_X for all compositional data. (a)–(d): difference between MORB and harzburgite for CFMAS-I, NCFMAS-X, NCFMAS-KT and NCFMAS-G, respectively. (e)–(h): difference between MORB and pyrolite for CFMAS-I, NCFMAS-X, NCFMAS-KT and NCFMAS-G, respectively. The black lines show the approximate location of the solidus (liquid phases are not included in our calculation). The unit of the color bars is a percent.

has temperature-, depth-, and yield stress-dependent viscosity. As in Xu et al. (2008), pyrolite is assumed to consist of a mechanical mixture of 80% harzburgite and 20% MORB. This is lower than the 30% MORB fraction assumed in our initial study (Nakagawa et al., 2009). The initial condition is an adiabatic temperature profile with error function thermal boundary layers at both boundaries and small random perturbations, and a uniform pyrolitic composition consisting of a mechanical mixture of 80% harzburgite and 20% MORB. Compositional anomalies are generated by melting and the formation of oceanic crust. The numerical procedure and resolution are the same as in our previous paper (Nakagawa et al., 2009), applying the Yin-Yang grid to model a 3-D spherical shell with $64\times192\times64\times2$ cells and 20 million tracers tracking composition. The model is designed to treat the evolution of the Earth, including decaying radiogenic heating and a CMB temperature decreasing with time based on a parameterized core heat balance (Nakagawa and Tackley, 2005a,b). To reach the age of Earth it is necessary to take 10,000 to 16,000 time steps. All physical parameters are also the same as our previous paper (see Table 1 in Nakagawa et al., 2009).

These parameters result in a convective vigor in which the surface velocity during the last 2 billion years fluctuates from ~2–6 cm/year and the surface heat flow is in the range 20–25 TW, the latter of which is lower than the inferred Earth's present-day instantaneous surface heat flow of

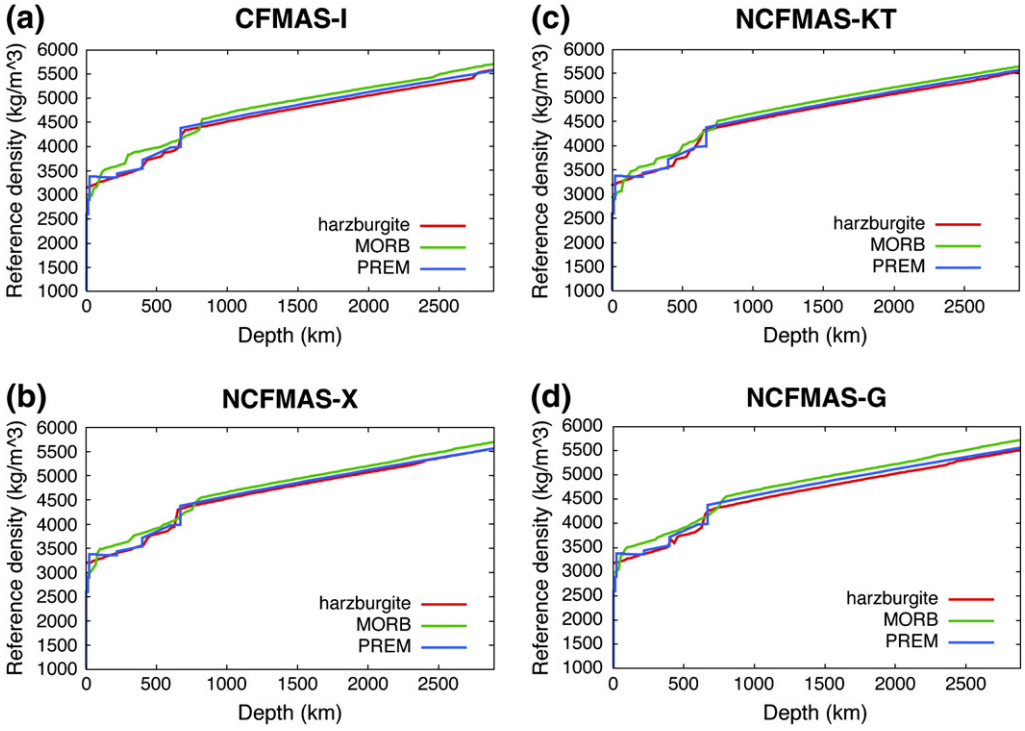

Fig. 2. Reference density profiles along the 1800 K isotherm for the four compositional models, compared to the density profile of PREM (Anderson and Dziewonski, 1981). (a) CFMAS-I. (b) NCFMAS-X. (c) NCFMAS-KT. (d) NCFMAS-G.

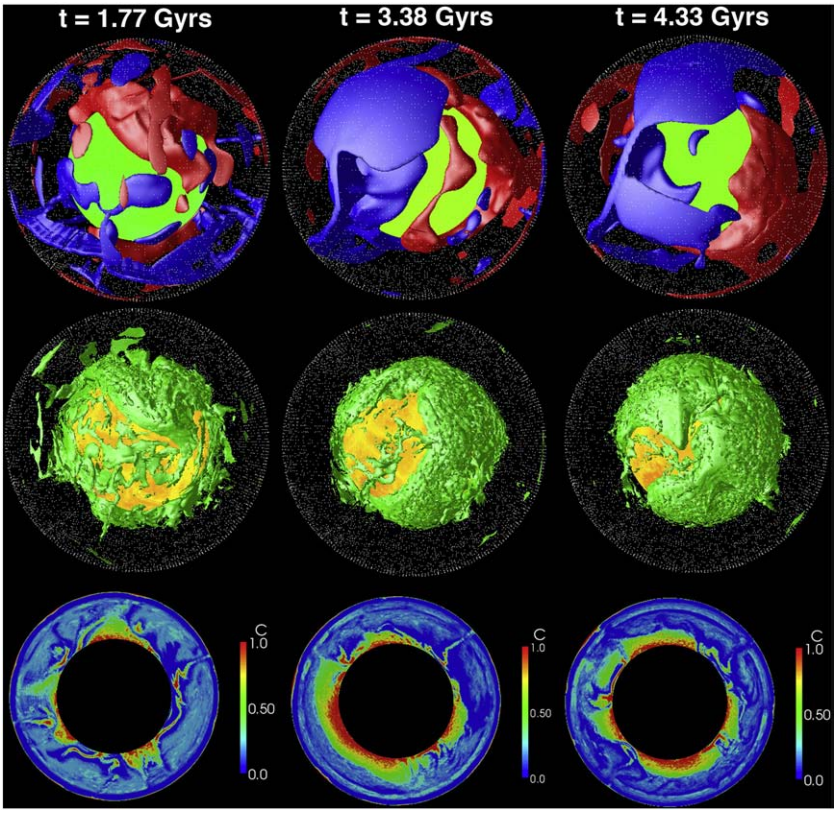

Fig. 3. Time variation of thermo-chemical structures for composition NCFMAS-X. Top row: Temperature residuals (red: 250 K hotter and blue: 250 K colder than the horizontally averaged temperature). Middle row: Compositional isosurface (75% basalt fraction). Bottom row: Equatorial slices of the compositional field.

46 TW (Jaupart et al., 2007), but this is a normal problem in evolution models.

4. Results

4.1. Thermo-chemical structures

Fig. 3 shows the time evolution of thermal and chemical structures for the case with the NCFMAS-X composition. Characteristic features are cold, compositionally-layered slab-like features (blue) reaching the CMB, and uneven accumulations of subducted MORB (green) above the CMB. The compositional anomalies in the deep mantle region are not as extensive or as distinct as in our previous study (Nakagawa et al., 2009), because there is less basaltic material in total (20% rather than the 30% assumed previously). Trapping of basalt in the transition zone due to the density crossover shown in Figs. 1 and 2 is visible in the second half of the model evolution. As pointed out in our previous papers, the trapped basalt does not peel directly off slabs as they sink through the transition zone (as modelled by van Keken et al., 1996), but rather it is basalt that has separated from the slab at the CMB, and later been entrained in mantle flow. The global structure is characterized at early times by a depleted upper mantle and a lower mantle that is mostly primitive but with basalt and harzburgite at the base, while at later times the mantle is generally depleted except for basalt enrichment near the CMB and in the transition zone.

Fig. 4 shows the thermal and chemical structures for the other three compositions, 4.5 Gyrs after the initial condition. The compositional structures in the CMB region are somewhat different for each composition. For all cases, the mantle is generally depleted except for basalt enrichment near the CMB and in the transition zone. The amount of basalt settling above the CMB increases from CFMAS-I to NCFMAS-KT to NCFMAS-G, with NCFMAS-X (Fig. 3) being most similar to NCFMAS-KT. Trapping of basalt above 660 km and harzburgite below 660 km is visible in all cases and displays the inverse trend to settling above the CMB, being most extensive than in the CFMAS-I case. For NCFMAS-KT (Fig. 4 b, e, and h), the amount of basalt segregation in the deep mantle is comparable to that of the NCFMAS-X case, as is trapping of basalt in the transition zone. For NCFMAS-G (Fig. 4 c, f, i), basaltic segregation in the deep mantle is extensive, forming a global layer, because the density difference between MORB and harzburgite is the largest of any of the compositions. There is little basaltic material trapped in the transition zone.

4.2. Compositional profiles

In order to quantify the strength of the 660 km basaltic filter and CMB basaltic segregation, it is useful to plot laterally-averaged one-dimensional compositional profiles, here shown in Fig. 5. The NCFMAS-X composition leads to the greatest basaltic filter effect, with CFMAS-I and NCFMAS-KT having a slightly lower effect and NCFMAS-G having the lowest effect. One reason for NCFMAS-G having the lowest basalt concentration in the transition zone is that most of the basalt has segregated above the CMB due to its high density (Fig. 4c). The other two NCFMAS compositions have less basalt segregation above the CMB and are similar to each other. For the five-component system there is less CMB basalt segregation, which is due to the effect of the post-perovskite transition in reducing the density anomaly of MORB in the deepest mantle (Figs. 1 and 2).

4.3. Seismological features

Using the Perple_X framework, elastic properties and seismic velocities may be calculated. These properties are directly evaluated for each pressure, temperature and composition, not evaluated using depth-dependent partial derivatives as often done in the past (e.g., Samuel et al., 2005; Tan and Gurnis, 2007; Deschamps and Tackley, 2009). This gives the possibility that properties may vary nonlinearly with temperature, although as compositional variations are treated as

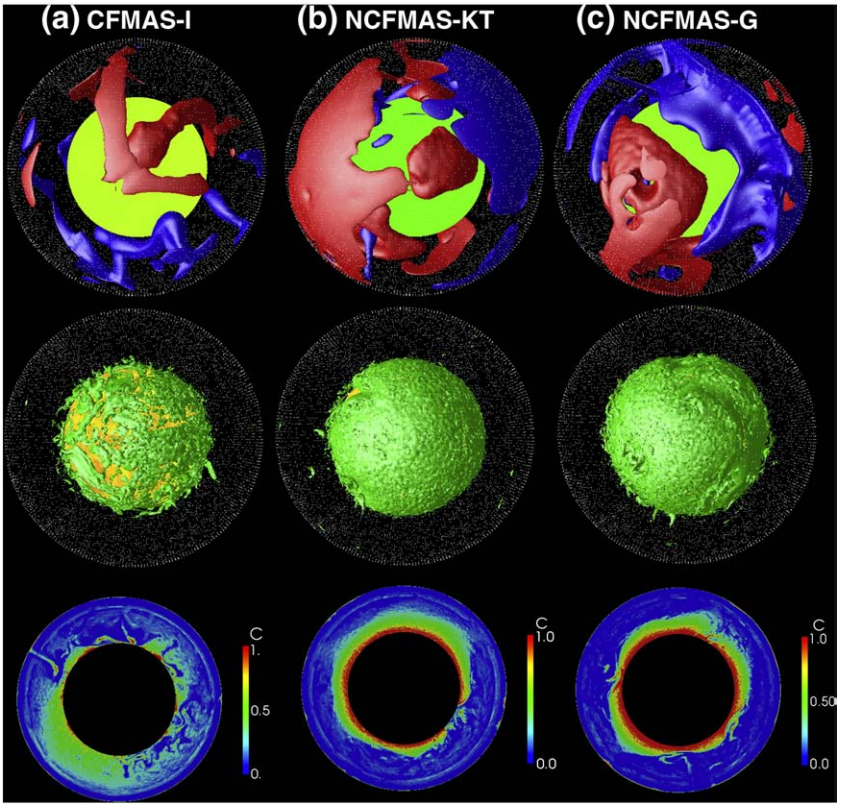

Fig. 4. Thermo-chemical structures at the final time snapshot for cases other than NCFMAS-X, i.e., CFMAS-I, NCFMAS-KT and NCFMAS-G.

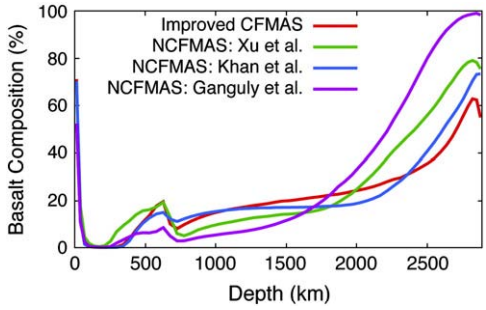

Fig. 5. Horizontally averaged compositional profiles.

mechanical mixing between two endmembers, properties vary linearly with composition.

Fig. 6 shows three-dimensional images and equatorial slices of shear-wave velocity anomalies (relative to the horizontal average) for the final frame of each case. In all cases, there is strong heterogeneity in the deep mantle, with fast anomalies (blue) in regions where subducted slabs impinge upon the CMB, and slow anomalies (red) in areas where basaltic layering builds up, which also become hot. This shows that despite MORB having a faster calculated shear-wave velocity than harzburgite, areas where basalt accumulates above the CMB are seismically slow because they are hot. The contrast between slow and fast anomalies appears to be lower for NCFMAS-X (b and f) and NCFMAS-KT (c and g) compositions, because the sensitivity of seismic velocity to temperature is lower. For the NCFMAS-G composition (d and h), seismic anomalies above the CMB are close to zero because dense basaltic layering is well-developed there and both thermal and compositional anomalies are very small in such a layer.

In order to statistically compare the synthetic velocity anomalies predicted by models of convection to global seismic tomography, we have plotted spectral heterogeneity maps (SHM) (Tackley et al., 1994) for the global averaged tomographic model SMEAN (Becker and Boschi, 2002) and those calculated from the convection models (Fig. 7). These show some systematic similarities and differences between tomography and synthetic anomalies from convection models, as well as differences between the synthetic anomalies. The dominance of long wavelength heterogeneity in Earth is reproduced by the convection models, but they appear to be too dominated by long wavelength heterogeneity, i.e., they have not enough short-wavelength heterogeneity. Convection models also reproduce the peak in heterogeneity in the upper ~200 km, with NCFMAS-KT displaying the most Earth-like upper mantle. Differences exist, however, in the deep mantle. In SMEAN there is a peak right at the CMB, whereas the convection models display peaks some distance above the CMB, with large-amplitude heterogeneity extending to 1500–1000 km depth. This extended peak in the lowermost mantle is caused by the presence of the compositional layering, as demonstrated in Tackley (2002). While this might suggest that a nearly isochemical deep mantle explains observations best (e.g., Schuberth et al., 2009), one of the first-order seismic observations of the deep mantle is an anti-correlation between bulk sound velocity and shear-wave anomalies, as well as an anti-correlation between shear-wave anomalies and density, which can only be explained by combined thermal and chemical variations (e.g. Trampert et al., 2004; Bull et al., 2009).

The thermal and compositional contributions to deep mantle seismic anomalies are plotted separately in Fig. 8. The 'temperature' SHM is obtained by setting composition everywhere to 20% basalt but using the model temperature field, whereas the 'composition' SHM is obtained by setting temperature to a reference adiabat but using the model composition. With CFMAS-I (Fig. 8 a,e,i), most of the heterogeneity in the deep mantle is due to thermal effects; the effect of composition on seismic anomalies is weaker, whereas with the other compositions, the contributions of temperature and composition to deep mantle heterogeneity have similar amplitudes. With NCFMAS-X (Fig. 8 b,f,j), temperature anomalies (Fig. 8 b) cause an eye-like structure in the mid lower mantle whereas compositional effects cause a similar amplitude peak extending from the CMB. With NCFMAS-KT (Fig. 8 c,g,k), the peak of temperature is again in the mid lower mantle, whereas compositional variations cause a peak at the CMB, which is closer to Earth-like. With NCFMAS-G (Fig. 8 d,h,l), the peak of temperature heterogeneity covers the entire lower mantle. In addition, compositional variations cause an eye-like structure because of lateral variations in the depth of the global basalt layer above the CMB (Tackley, 2002). For all of these, it is not surprising that the thermal heterogeneity is zero right at the CMB, because this is an isothermal boundary, at which there is zero lateral heterogeneity. If there really is lateral heterogeneity right at the CMB, which seismic tomographic models contain, then it must be caused by compositional variations. The post-perovskite phase transition is another contributor to lateral heterogeneity in the CMB region (Nakagawa and Tackley, 2005b, 2006), but this is not playing a major role in these calculations.

5. Discussion and conclusions

In the present study, we have investigated the sensitivity of thermo-chemical structures in the mantle to bulk MORB and harzburgite composition, with phase assemblages computed from four different sets of compositions using the principle of minimization of free energy. The main findings are as follows:

1) Small differences in the assumed composition of MORB (i.e., 1–2% differences in the oxide fractions) make a significant difference to the resulting thermo-chemical and seismically-observed structures. These differences arise because of differences in the MORB-harzburgite density contrast as a function of pressure and temperature (particularly as related to the density crossover below 660 km depth and the density contrast near the CMB) (Figs. 1 and 2) and because of differences in the scaling of seismic velocity with temperature and composition. The most important effects are related to the variations in the iron oxide fraction, which significantly influences density (see Figs. 1 and 2), and variations in the alumina oxide fraction. Using the more realistic six-oxide NCFMAS system that includes sodium rather than the five-oxide CFMAS system also causes differences, although substantial differences are also observed between the three NCFMAS compositions — in particular, the NCFMAS-G composition, which is based on older data, gives different physical properties to the other two. In Earth there is a natural variability in MORB composition, both at the present time (over the depth of the oceanic crust and between different spreading ridges) and over the age of the Earth due to mantle cooling changing the degree of melting and melting (temperature, pressure) conditions, which makes it difficult to draw clear quantitative conclusions about the dynamics. The depleted component in Earth also has a continuum of compositions, not considered here. These issues should be explored in detail in the future by considering a wider range of compositions than the four considered here.
2) The basalt filter effect, by which basalt tends to be trapped in the transition zone and harzburgite below the transition zone due to the different depths of the transition to perovskite (e.g., Ringwood and Irifune, 1988), is strongly affected by MORB composition. For CFMAS-I, NCFMAS-X and NCFMAS-KT, it is strong, but, for NCFMAS-G, it is almost non-existent because a huge amount of MORB is trapped at the CMB due to large density of MORB in that region. In any case, it is clear from the density anomaly maps (Fig. 1) that the depth extent of the density crossover depends on temperature, so it does not have much effect on cold slabs, and has the strongest effect on material that has warmed to the ambient mantle temperature or hotter. From an observational (e.g., seismological) perspective, it is not yet clear what compositional stratification exists around 660 km in Earth but some progress is being made, both in detailed seismic studies of lateral variability in seismic discontinuities (Andrews and Deuss, 2008;

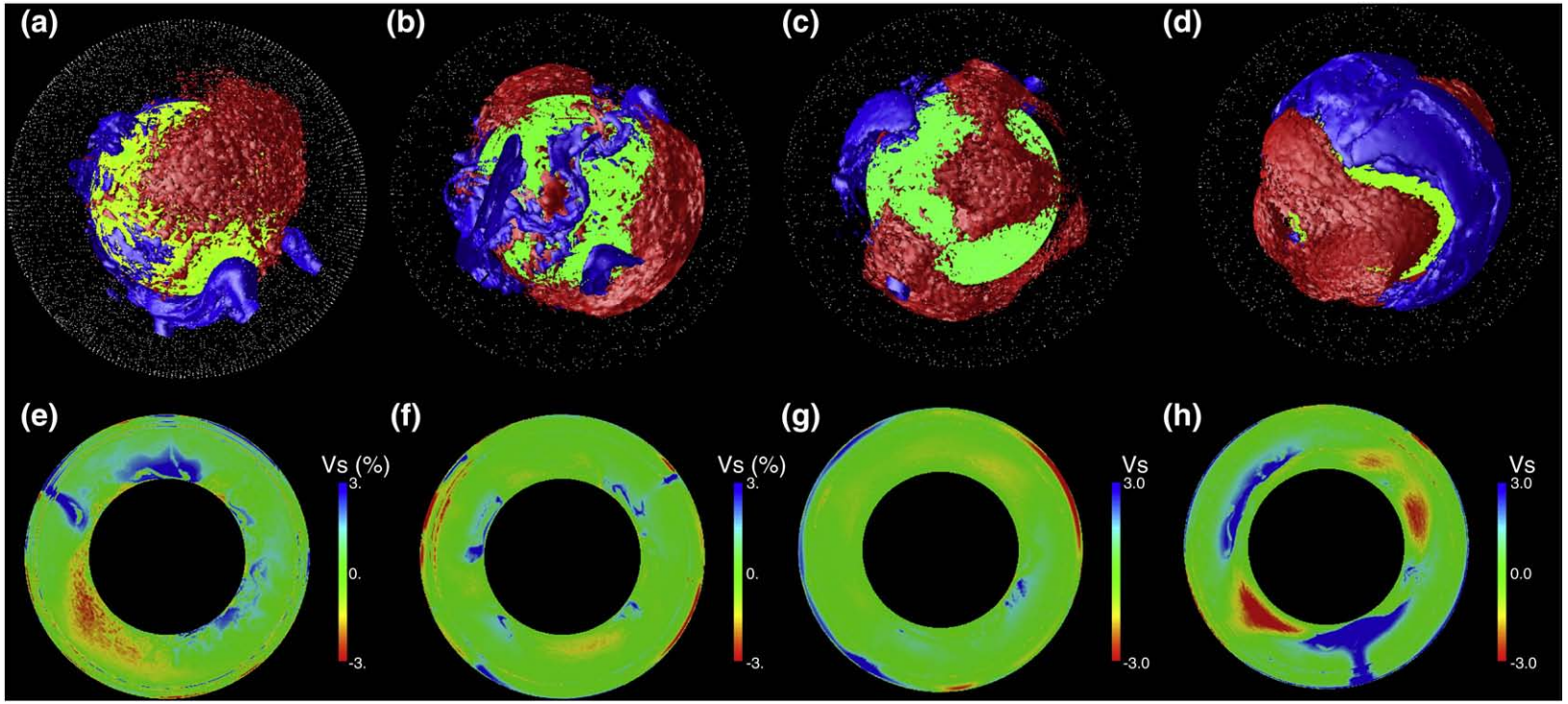

Fig. 6. Seismic anomalies in the lower mantle ((a)–(d); blue: +1 % and red: −1% anomalies) and their equatorial slices ((e)–(h)). (a) and (e); CFMAS-I. (b) and (f): NCFMAS-X. (c) and (g): NCFMAS-KT. (d) and (h): NCFMAS-G.

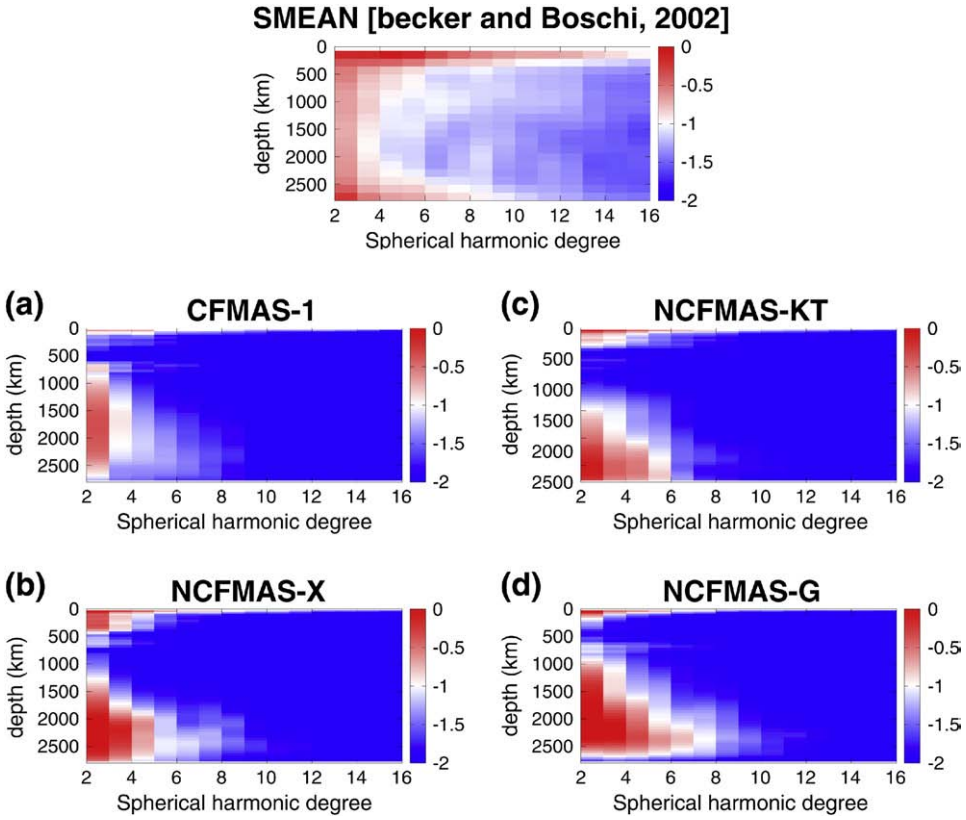

Fig. 7. Spectral heterogeneity maps for convection models compared to the mean seismic tomographic model SMEAN by Becker and Boschi (2002). (a) CFMAS-I, (b) NCFMAS-X, (c) NCFMAS-KT and (d) NCFMAS-G. Color bars indicate log10 of the power.

Deuss, 2009) and in stochastic inversions of surface wave data for profiles of temperature and composition (e.g., Cobden et al., 2008; Khan et al., 2009), both of which could potentially be compared to results from dynamical simulations such as the ones presented here.

3) The upper mantle is generally depleted except for the transition zone, which can be enriched as discussed in point 2. This is broadly consistent with the compositional profiles obtained in the 3-D stochastic inversions of surface wave data (Khan et al., 2009), in which the basalt fraction is very low for much of the upper mantle but in some areas increases with depth from about 500-600 km. It is also consistent with compositional structures obtained from 1-D forward waveform modeling (Cobden et al., 2008), that suggest a depleted upper mantle and top part of lower mantle but an enriched transition zone.
4) The upper mantle seismic spectra are not much affected by compositional model because they are dominated by temperature effects; however in the deep mantle, temperature and composition contribute roughly equally to seismic heterogeneity, except in the case with only a 5-oxide composition (CFMAS-I), in which composition has a much lower contribution. The model with NCFMAS-KT matches best the seismological model SMEAN both in amplitude and in dominant wavelengths, although no models fit the seismic models particularly well.
5) In the deep lower mantle, the amount of basalt segregation above the CMB and resulting deep mantle seismic velocity structure are influenced by the exact composition assumed. In general, basalt has a smaller density anomaly for NCFMAS-X and NCFMAS-KT than the CFMAS composition, although due to the effect of the post-perovskite transition the amount of layering is least in the CFMAS case. Again, for NCFMAS-G, deep mantle layering is strongest because of the relatively large FeO fraction. None of the numerical models are a good match to the seismic tomographic model SMEAN in the lower mantle, because although they are dominated by similarly long wavelengths, they have too much heterogeneity in the mid lower mantle caused by the chemical layering (Tackley, 2002). In general NCFMAS-KT matches best the SMEAN model, but strong heterogeneity is still too extended into the mid lower mantle. This implies that the amount of MORB layering is too much in these models, although the conclusion seems a little different when seismic models based on normal mode data are used (Deschamps and Tackley, 2008, 2009) which is under further investigation. However, some amount of compositional variation is still required, because although some features can be matched by purely thermal models (Schuberth et al., 2009), compositional variations are required to match the anti-correlation of shear and bulk sound wave velocities (Trampert et al., 2004; Bull et al., 2009) and also to obtain any lateral variations at all at the isothermal CMB. The question arises of why the amount of layering is overpredicted; possible answers include inaccurate mineralogical thermodynamic database, insufficient numerical resolution or too high deep mantle viscosity, and these need to be checked in the future.
6) The different compositions result in differences in the manifestation of the post-perovskite transition, which affect the resulting structure and dynamics according to our previous studies with parameterized phase boundaries (Nakagawa and Tackley, 2005a,b, 2006). In particular, at the conditions experienced in the lowermost mantle, post-perovskite in the MORB endmember only occurs with the CFMAS-I composition, which reduces its density anomaly. As the PPv transition is becoming increasingly constrained by ongoing experimental and theoretical mineral physics studies (e.g., Tateno et al., 2009; Tsuchiya and Tsuchiya, 2008), we should in future be able to adjust the thermodynamic data that goes into the Perple_X software, in order to match experimentally-determined pressures and properties. Characteristic features interpreted from both mineral physics and seismological images in the deep mantle (e.g. Garnero and McNamara, 2008) may then be reproduced more realistically.

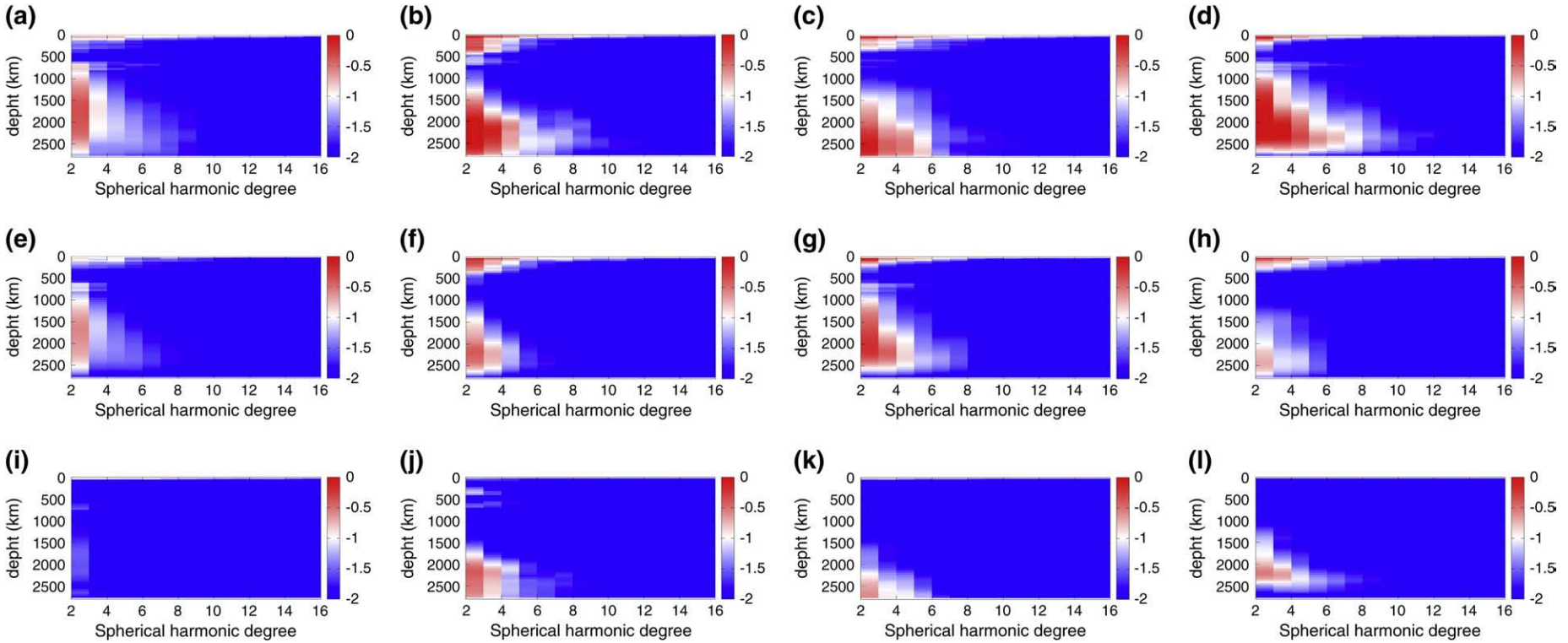

Fig. 8. Spectral heterogeneity maps for individual contributions: (a)–(d): total spectra. (e)–(h): temperature effects. (i)–(l): compositional effects. Left column: CFMAS-I. Left-center column: NCFMAS-X. Right-center column: NCFMAS-KT. Right column: NCFMAS-G. Color bars indicate log10 of power.

7) Regarding the treatment of plate tectonics and subduction, the visco-plastic yielding rheology used here appears to give similar results to simulations that use a force-balanced plates or an imposed plate velocity (Christensen and Hoffmann, 1994; Davies, 2002; Brandenburg et al., 2008). Both treatments result in thin basaltic crust and similar features in the deep mantle, with basaltic material accumulated above the CMB.

From the above discussions, future directions include (i) consideration of a broader range of MORB compositions arising from spatial and temporal variations, (ii) comparisons between convection models and seismic models in the transition zone, to constrain possible compositional layering, (iii) improvement of the deep mantle thermodynamic database, and (iv) more realistic physical parameters for the mantle convection modeling.

Acknowledgements

The authors thank Amir Khan on providing compositional data on MORB and discussions. All numerical simulations are performed on the Brutus cluster operated by the Informatiksdienst of ETH Zurich. Supported by SNF grant 200021-111870. We thank Peter van Keken, an anonymous reviewer and Lars Stixrude for constructive reviews.

References

Andrews, J., Deuss, A., 2008. Detailed nature of the 660 km region of the mantle from global receiver function data. J. Geophys. Res. 113. doi:10.1029/2007JB005111.
Baker, M.B., Beckett, J.R., 1999. The origin of abyssal peridotites: a reinterpretation of constraints based on primary bulk compositions. Earth Planet. Sci. Lett. 171, 49–61.
Becker, T., Boschi, L., 2002. A comparison of tomographic and geodynamic mantle models. Geochem. Geophys. Geosyst. 3. doi:10.1029/2001GC000168.
Brandenburg, J.P., van Keken, P.E., 2007. Deep storage of oceanic crust in a vigorously convecting mantle. J. Geophys. Res. 112, B06403. doi:10.1029/2006JB004813.
Brandenburg, J.P., Hauri, E.H., van Keken, P.E., Ballentine, C.J., 2008. A multiple-system study of the geochemical evolution of the mantle with force-balanced plates and thermochemical effects. Earth Planet. Sci. Lett. 276, 1–13.
Brown, G.C., Mussett, A.E., 1981. The Inaccessible Earth. George Allen and Unwin, London. 235 pp.
Bull, A.L., McNamara, A.K., Ritsema, J., 2009. Synthetic tomography of plume clusters and thermochemical piles. Earth Planet. Sci. Lett. 278, 152–162.
Christensen, U.R., Hofmann, A.W., 1994. Segregation of subducted oceanic crust in the convecting mantle. J. Geophys. Res. 99, 19867–19884.
Cobden, L., Goes, S., Cammarano, F., Connolly, J.A.D., 2008. Thermochemical interpretation of one-dimensional seismic reference models for the upper mantle: evidence for bias due to heterogeneity. Geophys. J. Int. 175, 627–648.
Connolly, J.A.D., 2005. Computation of phase equilibria by linear programming: a tool for geodynamic modeling and an application to subduction zone decarbonation. Earth Planet. Sci. Lett. 236, 524.
Davies, G., 2002. Stirring geochemistry in mantle convection models with stiff plates and slabs. Geochim. Cosmochim. Acta 66, 3125–3142.
Davies, G.F., 2008. Episodic layering of the early mantle by the 'basalt barrier' mechanism. Earth Planet. Sci. Lett. 275, 382–392.
Deschamps, F., Tackley, P.J., 2008. Searching for models of thermo-chemical convection that explain probabilistic tomography I. Principles and influence of rheological parameters. Phys. Earth Planet. Int. 171, 357–373.
Deschamps, F., Tackley, P.J., 2009. Searching for models of thermo-chemical convection that explain probabilistic tomography II — influence of physical and compositional parameters. Phys. Earth Planet. Int. 176, 1–18.
Dziewonski, A.M., Anderson, D.L., 1981. Preliminary reference Earth model. Phys. Earth Planet. Int. 35, 297–356.
Deuss, A., 2009. Global observations of mantle discontinuities using SS and PP precursors. Surv. Geophys. 30 (4), 301–326.
Ganguly, J., Freed, A.M., Saxena, S.K., 2009. Density profiles of oceanic slabs and surrounding mantle: integrated thermodynamic and thermal modeling, and implications for the fate of slabs at the 660 km discontinuity. Phys. Earth Planet. Int. 172, 257–267.
Garnero, E.J., McNamara, A.K., 2008. Structure and dynamics of Earth's lower mantle. Science 320, 626–628.
Hirose, K., Takafuji, N., Sata, N., Ohishi, Y., 2005. Phase transition and density of subducted MORB crust in the lower mantle. Earth Planet Sci. Lett. 237, 239–251.
Irifune, T., Ringwood, A.E., 1993. Phase transformations in subducted oceanic crust and buoyancy relationships at depths of 600–800 km in the mantle. Earth Planet Sci. Lett. 117, 101–110.
Ishii, M., Tromp, J., 1999. Normal-mode and free-air gravity constraints on lateral variations in velocity and density. Science 285, 1231–1236.
Jaupart, C., Labrosse, S., Marescal, J.-C., 2007. Heat and energy in the mantle of the Earth. Treatise of Geophysics. : Mantle dynamics, Vol. 7. Elsevier, pp. 253–303.
Khan, A., Boschi, L., Connolly, J.A.D., 2009. On mantle chemical and thermal heterogeneities and anisotropy as mapped by inversion of global surface wave data. J. Geophys. Res. 114, B09305. doi:10.1029/2009JB006399.
Lyubetskaya, T., Korenaga, J., 2007. Chemical composition of Earth's primitive mantle and its variance: 1 Method and results. J. Geophys. Res. 112, B03211. doi:10.1029/2005JB004223.
Nakagawa, T., Buffett, B.A., 2005. Mass transport mechanism between the upper and lower mantle in numerical simulations of thermochemical mantle convection with multicomponent phase changes. Earth Planet. Sci. Lett. 230, 11–27.
Nakagawa, T., Tackley, P.J., 2005a. Deep mantle heat flow and thermal evolution of the Earth's core based on thermo-chemical multiphase mantle convection. Geochem. Geophys. Geosyst. 6, Q08003. doi:10.1029/2005GC000967.
Nakagawa, T., Tackley, P.J., 2005b. The interaction between the post-perovskite phase change and a thermo-chemical boundary layer near the core–mantle boundary. Earth Planet Sci. Lett. 238, 204–216.
Nakagawa, T., Tackley, P.J., 2006. Three-dimensional structures and dynamics in the deep mantle: effects of post-perovskite phase change and deep mantle layering. Geophys. Res. Lett. 33. doi:10.1029/2006GL025719 L12S11.
Nakagawa, T., Tackley, P.J., Deschamps, F., Connolly, J.A.D., 2009. Incorporating self-consistently calculated mineral physics into thermochemical mantle convection simulations in a 3-D spherical shell and its influence on seismic anomalies in Earth's mantle. Geochem. Geophys. Geosyst. 10, Q3304. doi:10.1029/2008GC002280.
Ogawa, M., 2000. Numerical models of magmatism in convecting mantle with temperature-dependent viscosity and their implications for Venus and Earth. J. Geophys. Res. 105 (E3), 6997–7012.
Ogawa, M., 2003. Chemical stratification in a two-dimensional convecting mantle with magmatism and moving plates. J. Geophys. Res. 108, 2561. doi:10.1029/2002JB002205.
Ricard, Y., Mattern, E., Matas, J., 2005. Synthetic tomographic images of slabs form mineral physics. In: van der Hilst, R.D., Bass, J.D., Matas, J., Trampert, J. (Eds.), 'Earth's Deep Mantle' AGU Monograph Series, 160, pp. 283–300.
Ringwood, A.E., 1982. Phase-transformations and differentiation in subducted lithosphere — implications for mantle dynamics, basalt petrogenesis, and crustal evolution. J. Geol. 90, 611–643.
Ringwood, A.E., Irifune, T., 1988. Nature of the 650-km seismic discontinuity: implications for mantle dynamics and differentiation. Nature 331, 131–136.
Samuel, H., Farnetani, C.G., Andrault, D., 2005. Heterogeneous lowermost mantle: compositional constraints and seismological observables. In: van del Hilst, R.D., et al. (Ed.), Earth's Deep Mantle: Structure, Composition, and Evolution, Geophysical Monograph Series, 160. American Geophysical Union, pp. 101–116.
Schuberth, B.S.A., Bunge, H.-P., Steinle-Neumann, G., Moder, C., Oesser, J., 2009. Thermal versus elastic heterogeneity in high-resolution mantle circulation models with pyrolite composition: high plume excess temperatures in the lowermost mantle. Geochem. Geophys. Geosyst. 10. doi:10.1029/2008GC002235 Q01W01.
Stixrude, L., Lithgow-Bertelloni, C., 2005. Thermodynamics of mantle minerals — I. Physical properties. Geophys. J. Int. 162, 610–632. doi:10.1111/j.1365-246X.2005.02642.x.
Tackley, P.J., 2002. Strong heterogeneity caused by deep mantle layering. Geochem. Geophys. Geosyst. 3, 1024. doi:10.1029/2001GC000167.
Tackley, P.J., Stevenson, D.J., Glatzmaier, G.A., Schubert, G., 1994. Effects of multiple phase transitions in a 3-dimensional spherical model of convection in Earth's mantle: J. Geophys. Res. 99, 15877–15901.
Tackley, P.J., Xie, S., Nakagawa, T., Hernlund, J.W., 2005. Numerical and laboratory studies of mantle convection: philosophy, accomplishments and thermo-chemical structure evolution. In: van der Hilst, R.D., et al. (Ed.), 'Earth's Deep Mantle: Structure, Composition and Evolution', Geophys, Monogr. Ser., vol. 160. AGU, Washington D.C., pp. 83–99.
Takahashi, E., 1986. Melting of a dry peridotite KLB-1 up to 14 GPa: implications on the origin of peridotitic upper mantle. J. Geophys. Res. 91, 9367–9382.
Tan, E., Gurnis, M., 2007. Compressible thermochemical convection and application to lower mantle structures. J. Geophys. Res. B06304. doi:10.1029/2006JB004505.
Tateno, S., Hirose, K., Sata, N., Ohishi, Yasuo, 2009. Determination of post-perovskite phase transition boundary up to 4400 K and implications for thermal structure in D″ layer. Earth Planet. Sci. Lett. 130–136.
Taylor, S.R., Mclennan, S., 2008. Planetary Crusts: Their Composition, Origin and Evolution. Cambridge University Press, Cambridge, UK.
Trampert, J., Deschamps, F., Resovsky, F., Yuen, D.A., 2004. Probabilistic tomography maps chemical heterogeneities throughout the lower mantle. Science 310, 853–856.
Tsuchiya, J., Tsuchiya, T., 2008. Postperovskite phase equilibria in the $MgSiO_3$–Al_2O_3 system. Proc. Natl. Acad. Sci. U. S. A. 105, 19160–19164.
van Keken, P.E., Karato, S., Yuen, D.A., 1996. Rheological control of oceanic crust separation in the transition zone. Geophys. Res. Lett. 23, 1821–1824.
Weidner, D.J., Wang, Y., 1998. Chemical and Clapeyron induced buoyancy at the 660 km discontinuity. J. Geophys. Res. 103, 7431–7441.
Weinstein, S.A., 1992. Induced compositional layering in a convecting fluid layer by an endothermic phase-transition. Earth Planet. Sci. Lett. 113 (1–2), 23–39.
Workman, R.K., Hart, S.R., 2005. Major and trace element composition of the depleted MORB mantle (DMM). Earth Planet. Sci. Lett. 231, 53072.
Xu, W., Lithgow-Bertelloni, C., Stixrude, L., Ritsema, J., 2008. The effect of bulk composition and temperature on mantle seismic structure. Earth Planet. Sci. Lett. 275, 70–79.